# Multiple Carrier Agile Radar via Compressed Sensing

Tianyao Huang, Yimin Liu, Yonina C. Eldar, Xiqin Wang

***Abstract*—Frequency agile radar (FAR) is known to have excellent electronic counter-countermeasure performance [1]. Recently, compressed sensing (CS) based algorithms have been developed for joint range and Doppler estimation in FAR. To further improve the reconstruction performance, this paper suggests a waveform based on FAR, which we refer to as multiple carrier agile radar (MCAR). In MCAR, multiple carriers are transmitted in each pulse. The mutual coherence of the measurement matrix of MCAR is analyzed, and is shown to be better than the counterpart of FAR. Numerical simulations also demonstrate the performance improvement of MCAR over traditional FAR using CS techniques in terms of probabilities of successful recovery.**

## I. Introduction

With the rapid development of electronic countermeasures techniques as well as the booming quantity of commercial electronic devices, the electromagnetic spectrum is increasingly congested and constrained. Countering these threats of complex electromagnetic environments has becomes a vital issue in radar systems.

Frequency agile radars (FARs), which randomly change the carrier frequencies of each pulse over time (see Fig. 1), are known to have good electronic counter-countermeasures (ECCM) performance [1] and have attracted considerable attention [2]–[6]. Frequency agility makes the radar pulses difficult to track and predict, and thus serves well in protecting the radar.

To jointly estimate the high range resolution (HRR) profile and Doppler of targets using FAR, compressed sensing (CS) methods [10] are usually preferred rather than the simpler matched filter. In matched filter, FAR suffers from sidelobe pedestal problems and weak targets could be masked by the sidelobe. By exploiting the sparsity of targets, CS methods alleviate the sidelobe pedestal problem and better estimate the range and Doppler parameters. In the noiseless case, CS methods guarantee to reconstruct $O\left(\sqrt{\frac{N}{\ln MN}}\right)$ scatterers [7], where $N$ is the number of pulses and $M$ is the number of HRR bins inside a low range resolution (LRR) bin. However, in complex electromagnetic environments, the radar encounters severe jamming and many pulse returns are lost. The recovery performance of FAR with a matched filter or CS decreases significantly in this case.

In order to improve the reconstruction performance in complex electromagnetic environments, this paper proposes a new transmission approach referred to as multiple carrier agile radar (MCAR). In this technique, multiple monotones (instead of a single one in FAR) are transmitted in each pulse (see Fig. 1). The echo of each monotone is received individually, which increases the number of measurements. When many pulses are lost, MCAR has more available measurements than FAR, and thus may improve the recovery performance. Following [7], we derive theoretical estimation performance guarantees for MCAR, and simulations are executed to validate its advantages.

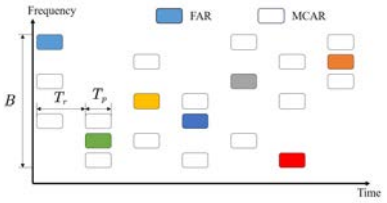


Fig. 1. An example of FAR/MCAR waveform. Filled blocks represent pulses of FAR. Unfilled blocks sketch pulses of MCAR.

The rest of paper is organized as follows. Section II introduces the signal model of MCAR. Section III briefly reviews CS methods and theoretically analyzes performance guarantees for MCAR. Numerical experiments are shown in Section IV and Section V concludes the paper.

## II. Signal Model

### A. Transmission Model

In each pulse of MCAR, multiple monotones are transmitted. The $\omega$-th monotone of the $n$-th transmitted pulse is written as

$$s_{n,\omega}(t) := A_{n,\omega}\text{rect}\left(\frac{t-nT_r}{T_p}\right)e^{j2\pi f_{n,\omega}(t-nT_r)}, \quad (1)$$

where $A_{n,\omega}$ is the amplitude, $n = 0, 1, \ldots, N-1$, $T_p$ is the pulse duration, and $T_r$ is the pulse repetition interval. The envelope of the pulse is assumed to be a rectangular function defined as

$$\text{rect}(x) := \begin{cases} 1, & 0 \le x \le 1, \\ 0, & \text{otherwise}, \end{cases} \quad (2)$$

and $f_{n,\omega}$ is the carrier frequency. The frequency is random in a specific band, $[f_c, f_c + B]$, specifically,

$$f_{n,\omega} = f_c + d_{n,\omega}B, \quad (3)$$

where $f_c$ is the initial frequency, $d_{n,\omega}$ is the corresponding frequency modulation code, which is a random variable, $d_{n,\omega} \in [0, 1)$, and $B$ is the synthetic bandwidth.

We assume that the code $d_{n,\omega}$ is chosen from the discrete set $\mathcal{D}_d := \{\frac{m}{M} | m=0,1,\ldots,M-1\}$, and each element in $\mathcal{D}_d$ has the same probability to be selected. We denote $\Omega_n$ by the

set including the random modulation codes chosen for the $n$-th pulse,

$$\Omega_n := \{d_{n,\omega} | \omega = 0, 1, \dots P\}, \tag{4}$$

where $P$ is the number of carriers in each pulse, i.e., $P := |\Omega_0| = |\Omega_1| = \cdots = |\Omega_{N-1}|$.

Summing up all the monotones yields the $n$-th transmission

$$s_n(t) := \sum_{\omega=0}^{P-1} s_{n,\omega}(t). \tag{5}$$

For each pulse, the whole transmission power is constrained and equally distributed to selected carriers. Thus

$$A_{n,\omega} = \frac{1}{\sqrt{P}}. \tag{6}$$

FAR is a special case of MCAR with $P = 1$.

### *B. Return Model of Single Scatterer*

In MCAR, the returns of different monotones are received and processed separately, and are assumed to be delays of the transmitted pulses. Consider an ideal point scatterer with scattering coefficient $\beta \in \mathbb{C}$, at range $r$. The return of the $n$-th pulse, $\omega$-th carrier is

$$R_{n,\omega}(t) := \beta s_{n,\omega}\left(t - \frac{2r}{c}\right). \tag{7}$$

If the scatterer is moving away from the radar with a relative radial velocity $v$, then the range is a function of time $t$, $r(t) = r(0) + vt$, and (7) can be rewritten as

$$R_{n,\omega}(t) = \beta/\sqrt{P}\mathrm{rect}(\xi) e^{j2\pi f_{\omega,n}(t - nT_r - \tau - 2vt/c)}, \tag{8}$$

where $\xi := (t - nT_r - \tau - 2vt/c)/T_p$ and $\tau := 2r(0)/c$ for brevity. After demodulation with $e^{j2\pi f_{n,\omega}(t-nT_r)}$ and normalization with $1/\sqrt{P}$, the echo is represented by

$$\tilde{R}_{n,\omega}(t) = \beta \mathrm{rect}(\xi) e^{j2\pi f_{n,\omega}(-\tau - 2vt/c)}. \tag{9}$$

We sample the echoes at the Nyquist rate of $f_s = 1/T_p$ so that there is one sample for each pulse. Each sampling instant corresponds to a LRR bin. Measurements in the same time instance are then as

$$\boldsymbol{y}(t) = [\tilde{R}_{0,0}(t), \tilde{R}_{0,1}(t), \dots, \tilde{R}_{n,\omega}(t + nT_r), \dots]^T, \tag{10}$$

and processed to provide a refined range, i.e. HRR range, and Doppler. In this paper, we focus on joint HRR range and Doppler estimation.

The sampling instant $t_{n,l} = nT_r + l/f_s$ captures echoes from scatterers located in the $l$-th LRR bin, $r \in [l-1, l]\Delta_{\mathrm{L}}$, $l = 1, 2, \dots, \lfloor T_r f_s \rfloor$, where $\Delta_{\mathrm{L}} := T_p c/2$ representing the LRR. Since measurements from all LRR bins are processed identically, without loss of generality, we can take any LRR bin as an example. Assume that the $l$-th LRR bin contains the scatterer and $\mathrm{rect}(\xi)|_{t=t_{n,l}} = 1$. Substituting $t = t_{n,l}$ into (9), we have

$$\begin{aligned} \tilde{R}_{n,\omega}(t_{n,l}) &= \beta e^{-j4\pi(f_c + d_{n,\omega}B)(r(0) + v(nT_r + l/f_s))/c} \\ &\approx \tilde{\gamma} e^{-j4\pi d_{n,\omega} B r(0)/c} e^{-j4\pi f_c v T_r n \zeta_{n,\omega}/c}, \end{aligned} \tag{11}$$

where $\tilde{\gamma} := \beta e^{-j4\pi f_c \frac{r(0) + vl/f_s}{c}}$, $\zeta_{n,\omega} := 1 + d_{n,\omega}B/f_c$, and the approximation is based on the assumption that $e^{-j4\pi d_{n,\omega} Bvl/(f_s c)} \approx 1$, which means that the relative motion of the scatterer during the wave propagation ($l/f_s$) is negligible, i.e. $\frac{vl/f_s}{c/(2B)} < \frac{vT_r}{c/(2B)} \approx 0$.

For brevity, we introduce $\tilde{p} := -4\pi B r(0)/(Mc)$, $\tilde{q} := -4\pi f_c v T_r/c$, and omit the notation $t_{n,l}$. Then (11) becomes

$$\tilde{R}_{n,\omega} \approx \tilde{\gamma} e^{j\tilde{p} M d_{n,\omega} + j\tilde{q} n \zeta_{n,\omega}}, \tag{12}$$

where $\tilde{\gamma}$, $\tilde{p}$ and $\tilde{q}$ are unknown. With the stacked measurements for $n = 0, 1, \dots, N-1$, $\omega = 0, 1, \dots, P-1$, we obtain the estimates $\hat{\gamma}$, $\hat{p}$ and $\hat{q}$. We then infer $|\hat{\beta}| = |\hat{\gamma}|$, $\hat{r}(0) = -\frac{Mc\hat{p}}{4\pi B}$ and $\hat{v} = -\frac{c\hat{q}}{4\pi f_c T_r}$, respectively.

Note that the HRR , $\Delta_{\mathrm{H}} := c/(2B)$, relies on the synthetic bandwidth. A LRR bin contains $M_*$ HRR bins, i.e.,

$$M_* := \left\lfloor \frac{T_p c}{2} \cdot \frac{2B}{c} \right\rfloor = \lfloor T_p B \rfloor \in \mathbb{N}. \tag{13}$$

To avoid grating lobes of the HRR profiles [8], [9], the minimum gap between frequency codes is required to satisfy $\min_{\omega_1 \neq \omega_2} |d_{n,\omega_1} - d_{n,\omega_2}| \leq 1/M_*$, which suggests a typical choice of $M = M_*$.

### *C. Return Model of Multiple Scatterers*

Assume that there are $K$ scatterers with parameters $(\tilde{\gamma}_k, \tilde{p}_k, \tilde{q}_k)$ corresponding to the same sampling instant (in the same LRR bin), $k = 0, 1, \dots, K-1$. Radar returns are cast as a summation of returns from all scatterers,

$$\tilde{R}_{n,\omega} = \sum_{k=0}^{K-1} \tilde{\gamma}_k e^{j\tilde{p}_k M d_{n,\omega} + j\tilde{q}_k n \zeta_{n,\omega}}. \tag{14}$$

We can rewrite the returns in matrix form. The measurements are represented by a vector $\boldsymbol{y} \in \mathbb{C}^{NP}$ with its $(nP + \omega)$-th entry as $\tilde{R}_{n,\omega}$, $n = 0, 1, \dots, N-1$, $\omega = 0, 1, \dots, P-1$.

The coefficients $\tilde{\gamma}$ will also be presented by a sparse vector. The resolutions of parameters $\tilde{p}, \tilde{q}$ are $1/M$ and $1/N$, respectively, and the unambiguous continuous region is $(p, q) \in [0, 2\pi)^2$. The $p, q$ parameters are divided into discrete grids according to the resolutions, respectively. Denote grid sets as $\mathcal{P} := \{\frac{2\pi m}{M} | m = 0, 1, \dots, M-1\}$ and $\mathcal{Q} := \{\frac{2\pi n}{N} | n = 0, 1, \dots, N-1\}$, respectively, and assume that parameters of scatterers precisely match grids in the sets $\mathcal{P}$ and $\mathcal{Q}$. Then $\tilde{\gamma}$ can be included in the matrix $\boldsymbol{X} \in \mathbb{C}^{M \times N}$ with entries

$$[\boldsymbol{X}]_{m,n} = \begin{cases} \tilde{\gamma}_k, \text{ if } \exists k, \ (\tilde{p}_k, \tilde{q}_k) = (p_m, q_n), \\ 0, \text{ otherwise.} \end{cases} \tag{15}$$

Vectorize $\boldsymbol{X}$ as $\boldsymbol{x} := \mathrm{vec}(\boldsymbol{X}^T) \in \mathbb{C}^{MN}$ with $[\boldsymbol{x}]_{n+mN} := [\boldsymbol{X}]_{m,n}$, and we obtain a matrix-form signal model as

$$\boldsymbol{y} = \boldsymbol{\Phi}\boldsymbol{x}, \tag{16}$$

where the $(nP + \omega, l + mN)$-th element of $\boldsymbol{\Phi} \in \mathbb{C}^{NP \times MN}$ is given by

$$[\boldsymbol{\Phi}]_{nP+\omega, l+mN} := e^{jp_m M d_{n,\omega} + jq_l n \zeta_{n,\omega}}, \tag{17}$$

$\omega = 0, 1, \ldots, P-1$, $m = 0, 1, \ldots, M-1$ and $l, n = 0, 1, \ldots, N-1$. If there are noises $\boldsymbol{w} \in \mathbb{C}^{NP}$, (16) becomes

$$\boldsymbol{y} = \boldsymbol{\Phi}\boldsymbol{x} + \boldsymbol{w}, \tag{18}$$

where $\boldsymbol{y}$ and $\boldsymbol{\Phi}$ are known, and $\boldsymbol{x}$ is to estimate. Since $d_{n,\omega}$ involved in $\boldsymbol{\Phi}$ is random, $\boldsymbol{\Phi}$ is random. After we solve $\boldsymbol{x}$, the $(p, q)$ parameters are then inferred from the support set of $\boldsymbol{x}$.

## III. Algorithms and Performance

In this section, we will discuss algorithms to solve the linear regression problems (16) and (18), and then theoretically analyze the performance of the methods. The result shows that MCAR has stronger performance guarantees than FAR.

### A. Review of Compressed Sensing Algorithms

In there are only a few scatterers inside a LRR bin, which means that $\boldsymbol{x}$ is sparse, and CS algorithms [10] can be used to reconstruct $\boldsymbol{x}$.

Basic pursuit finds the sparsest solution by

$$\min_{\boldsymbol{x}} \|\boldsymbol{x}\|_1, s.t.\ \boldsymbol{y} = \boldsymbol{\Phi}\boldsymbol{x}. \tag{19}$$

To reduce computational burden, greedy methods are often preferred. Typical examples include Subspace Pursuit and Iterative Hard Threshold.

It has been an important topic to theoretically analyze the conditions that guarantee correct recovery. Among these conditions, mutual coherence of the measurement matrix $\boldsymbol{\Phi}$ is easy to verify and widely used, and is defined as

$$\mu(\boldsymbol{\Phi}) := \max_{l \neq k} \frac{\left|\boldsymbol{\Phi}_l^H \boldsymbol{\Phi}_k\right|}{\|\boldsymbol{\Phi}_l\|_2 \|\boldsymbol{\Phi}_k\|_2}. \tag{20}$$

Theorem 1 provides a performance guarantee in the noiseless case.

**Theorem 1** ( [10]). *If the mutual coherence of $\boldsymbol{\Phi}$, $\mu(\boldsymbol{\Phi}) < \frac{1}{2K-1}$, then for any $\boldsymbol{x}$ with less than $K$ nonzeros, $\boldsymbol{x}$ is the unique solution to (19).*

The condition can be extended to robust recovery in noisy cases and also recovery using different CS methods.

### B. Performance Guarantee for MCAR

This subsection analyzes the mutual coherence of $\boldsymbol{\Phi}$ and proposes theoretical bounds for MCAR to guarantee correct recovery. The results show that it is easier for MCAR than FAR to meet the mutual coherence condition in Theorem 1. The mutual coherence relies on radar parameters, such as the number of pulses $N$ and choice of modulation code sets $\Omega_0$, $\Omega_1$, ..., $\Omega_{N-1}$. Since the code $d_{n,\omega}$ is random, $\boldsymbol{\Phi}$ is a random matrix. In the following, we will present a sufficient condition for radar parameters such that $\mu(\boldsymbol{\Phi}) < \frac{1}{2K-1}$ with high probability. We assume that the code sets $\Omega_n$ of each pulse are independent from each other, $n = 0, 1, \ldots, N-1$. Proofs are omitted due to space limitation.

Define the modulus $\boldsymbol{G} \in \mathbb{R}^{MN \times MN}$ with entries

$$[\boldsymbol{G}]_{k,l} = \left| \left[\boldsymbol{\Phi}^H \boldsymbol{\Phi}\right]_{k,l} \right|, k, l = 0, 1, \ldots, MN-1. \tag{21}$$

We then have the following result.

**Lemma 2.** *The rows of $\boldsymbol{G}$ are permutations of each other.*

Any row of $\boldsymbol{G}$ is therefore enough to analyze the mutual coherence. Take the 0-th row for convenience. Consider the $i$-th entry, corresponding to the $i$-th column of $\boldsymbol{\Phi}$, $\boldsymbol{\Phi}_i$. Recall that each column of $\boldsymbol{\Phi}$ has distinct parameters $(p, q)$. For brevity, we simply use the notation $(p, q)$ for $\boldsymbol{\Phi}_i$. Define

$$\chi_i := \frac{1}{NP} \boldsymbol{\Phi}_0^H \boldsymbol{\Phi}_i = \frac{1}{NP} \sum_{n=0}^{N-1} \sum_{\omega=0}^{P-1} e^{jpMd_{n,\omega} + jqn}, \tag{22}$$

$i = 1, 2, \ldots, MN-1$. The mutual coherence (20) becomes

$$\mu = \max_i |\chi_i|, i = 1, 2, \ldots, MN-1. \tag{23}$$

Generally, $\chi_i$ is random because $d_{n,\omega}$ is random. However, when $p = 0$ and $q \neq 0$, or equivalently $i \in \{1, 2, \ldots, N-1\}$, $\chi_i$ reduces to a constant variable,

$$\chi_i = \frac{1}{NP} \sum_{n=0}^{N-1} \sum_{\omega=0}^{P-1} e^{jqn} = 0. \tag{24}$$

In the rest of this subsection, we ignore these non-random $\chi_i$, which do not affect $\mu$. Denote a set

$$\Xi := \{N, N+1, \ldots, NM-1\}, \tag{25}$$

and we analyze $\chi_i$, $i \in \Xi$, where non-random values are excluded. We obtain the asymptotic statistic behavior as follows.

**Lemma 3.** *As $N \to \infty$, the real and imaginary parts of $\chi_i$, $\mathrm{Re}(\chi_i)$ and $\mathrm{Im}(\chi_i)$, $i \in \Xi$, have a joint Gaussian distribution,*

$$\begin{bmatrix} \mathrm{Re}(\chi_i) \\ \mathrm{Im}(\chi_i) \end{bmatrix} \sim \mathcal{N}\left( \begin{bmatrix} 0 \\ 0 \end{bmatrix}, \begin{bmatrix} \frac{1}{2NP} & 0 \\ 0 & \frac{1}{2NP} \end{bmatrix} \right), \tag{26}$$

*except in the special case that the corresponding parameters $p = q = \pi$, where the joint Gaussian distribution becomes*

$$\begin{bmatrix} \mathrm{Re}(\chi_i) \\ \mathrm{Im}(\chi_i) \end{bmatrix} \sim \mathcal{N}\left( \begin{bmatrix} 0 \\ 0 \end{bmatrix}, \begin{bmatrix} \frac{1}{2NP} & 0 \\ 0 & 0 \end{bmatrix} \right). \tag{27}$$

Lemma 3 is derived from the Lyapunov's central limit theorem. Since $\chi_i$ is an asymptotic Gaussian, the modulus $|\chi_i|$ obeys a Rayleigh distribution and we have the following corollary.

**Corollary 4.** *When $N \to \infty$ and $i \in \Xi$,*

$$\mathbb{P}(|\chi_i| > \epsilon) \leq e^{-NP\epsilon^2}. \tag{28}$$

Applying the union bound, we obtain Lemma 5.

**Lemma 5.** *As $N \to \infty$, the maximum, $\mu_m = \max_i |\chi_i|$, $i \in \Xi$, satisfies the following*

$$\mathbb{P}(\mu_m > \epsilon) \leq (MN - N) e^{-NP\epsilon^2}. \tag{29}$$

Lemma 5 shows that the mutual coherence can be bounded with certain probabilities. Theorem 1 indicates that $\mu(\boldsymbol{\Phi}) < \frac{1}{2K-1}$ leads to exact recovery. Substituting $\epsilon = \frac{1}{2K-1}$ into (29), we obtain the following theorem.

**Theorem 6.** *Given a constant $\delta \in (0,1)$, the mutual coherence satisfies $\mu(\mathbf{\Phi}) < \frac{1}{2K-1}$ with probability no less than $1-\delta$, if*

$$K \leq \frac{\sqrt{P}\mu_* + 1}{2}, \tag{30}$$

*where*

$$\mu_* = \sqrt{\frac{N}{\ln(MN-N) - \ln\delta}}. \tag{31}$$

In noisy cases, assume that the noise disturbing $R_{n,\omega}$ in (7) obeys a circularly symmetric complex Gaussian $\mathbb{CN}(\mathbf{0}, \sigma^2\boldsymbol{I})$. After normalization with $1/\sqrt{P}$, the noise behaves as $\boldsymbol{w} \sim \mathbb{CN}(\mathbf{0}, P\sigma^2\boldsymbol{I})$. Assume that $\|\boldsymbol{w}\|_2 \leq \epsilon_1 := C_1\sqrt{NP}\sigma$, and solve (18) using

$$\min_{\boldsymbol{x}} \|\boldsymbol{x}\|_1, s.t. \ \|\boldsymbol{y} - \mathbf{\Phi}\boldsymbol{x}\|_2 \leq \epsilon_2, \tag{32}$$

with $\epsilon_2 := C_2\sqrt{NP}\sigma$, where $C_1 < C_2$ are constants that do not depend on $N$, $P$ or $\sigma$. Combining with Theorem 6 and Theorem 2.1 in [11], we have the following corollary.

**Corollary 7.** *Let $\hat{\boldsymbol{x}}$ be the solution of (32). Then the error is bounded as*

$$\|\hat{\boldsymbol{x}} - \boldsymbol{x}\|_2 \leq \frac{\sqrt{3\left(1+\sqrt{P}\mu_*\right)}}{1-(2K-1)\sqrt{P}\mu_*}(C_1+C_2)\sqrt{NP}\sigma, \tag{33}$$

*with probability no less than $1-\delta$.*

In noiseless cases, MCAR can recover at least $K = O\left(\sqrt{\frac{NP}{\ln MN}}\right)$ scatterers, while the counterpart of traditional FAR is $K' = O\left(\sqrt{\frac{N}{\ln MN}}\right)$. Owing to the increased number of carriers of each pulse, there are more measurements for MCAR than FAR, which suggests better reconstruction performance. In noisy cases, the error bound is generally not monotonically decreasing along with the increase of $P$. In the next section, numerical experiments are executed to evaluate the practical performance.

## IV. Simulations

In this section, we perform simulations and compare the reconstruction performance of both the proposed MCAR and the traditional FAR.

Noiseless and noisy cases are considered. In each case, we focus on the performance under jamming environments, where partial returns are ruined. Assume that there are two kinds of jams, wideband jam and narrowband jam, marked as 'JamW' and 'JamN', respectively. Wideband jam occupies a large band such that returns of all carriers in a pulse are destroyed; see Fig. 2. Narrowband jam aims at some certain carriers in each pulse, so parts of returns in a pulse can survive; see Fig. 3. Assume that both jams saturate the receiver and are detected by the radar. It is known which pulse/carrier is ruined. Note that for FAR with only one carrier in each pulse, these two jam patterns are the same.

For the wideband jam, we define the pulse missing rate, $r_p$, as the number of ruined pulses divided by the number of transmitted pulses, $N$. For the narrowband jam, we define carrier missing rate, $r_c$, as the number of ruined carriers divided by the number of transmitted carriers, $NP$.

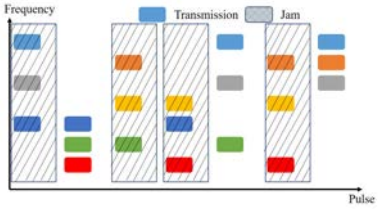


Fig. 2. Wideband jam. Once a pulse is jammed, all the carriers are jammed and ruined.

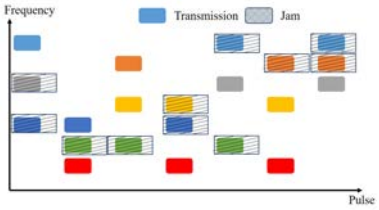


Fig. 3. Narrowband jam. Once a pulse is jammed, parts of the carriers are jammed and ruined.

### A. Noiseless Cases

We set that the initial frequency as $f_c = 10$ GHz, the synthetic bandwidth $B = 64$ MHz, the number of pulses $N = 48$ and the number of available carriers $M = 8$. For MCAR, the number of monotones in a pulse is set as $P = 3$. FAR can be considered as a special case of MCAR with $P = 1$. The number of scatterers $K$ are varied from 1 to 32. In each trial, the support set of $\boldsymbol{x}$, i.e. the set that indexes the locations of the nonzeros in $\boldsymbol{x}$, is randomly changed, which means the range and Doppler parameters of the scatterers are randomized. The amplitudes of scattering coefficients are all set as 1 and the phases are random obeying uniform distribution $U([0, 2\pi))$. One hundred Monte-Carlo trials are performed. We recover $\boldsymbol{x}$ by $\ell_1$ optimization using CVX [12], [13], and evaluate the probabilities of the event that the support set of $\boldsymbol{x}$ is exactly recovered.

We also test the reconstruction performance of MCAR and FAR under jamming environments. Assume under wideband and narrowband jams, that some pulses and carriers are randomly missed, respectively. The pulse missing rate and the carrier missing rate are $r_p = r_c = 0.5$.

The results are depicted in Fig. 4. Results show that MCAR dramatically outperforms FAR, in both cases with and without jams. The wideband and narrowband jams, which lead to the same missing rate, have similar impact on MCAR. These results indicate that the number of measurements play a key role on the reconstruction performance. MCAR transmits multiple carriers in each pulse, which significantly increases the number of measurements and the mutual coherence property of the measurement matrix, and thus improves the reconstruction performance of CS methods.

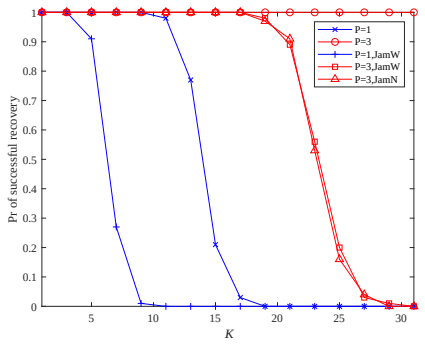


Fig. 4. Probabilities of support set exact recovery using (19) in noiseless cases.

In noiseless cases, when the mutual coherence $\mu < \frac{1}{2K-1}$, the scatterers' parameters are exactly recovered. According to (31), CS methods promise to recover at least $K = 2.6$ and $K = 1.7$ scatterers with probability higher than 0.9 for MCAR and FAR, respectively. However, compared with the simulation results, the theoretical bounds are quite pessimistic.

### B. Noisy Cases

The number of pulses is set to $N = 48$. The number of scatterers $K$ is fixed as 10, which is assumed known a priori. The variance of the noise disturbing $R_{n,\omega}$ in (7), $\sigma^2$, is changed from -15 dB to 15 dB. Two thousand Monte-Carlo trials are performed. The rest settings are the same as those in previous subsection.

We use Subspace Pursuit to estimate $\boldsymbol{x}$, and evaluate whether the support set of $\boldsymbol{x}$ is exactly recovered. The probabilities of exact recovery are shown in Fig. 5.

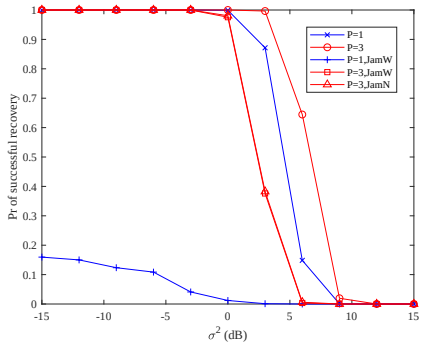


Fig. 5. Probabilities of support set exact recovery using Subspace Pursuit in noisy cases.

When there is no jam, the reconstruction performance of MCAR is better than that of FAR, but the improvement is not significant. When there are jams and missing pulses or carriers, MCAR dramatically outperforms FAR. Performance of MCAR under the two jamming patterns is very close. In the case without jams, the number of measurements is enough, and the signal to noise ratio (SNR, defined as $\sum_{\omega=0}^{P-1} A_{n,\omega}^2/\sigma^2$) rather than the number of measurements plays the key role. Compared with FAR, MCAR increases the number of measurements while keeping the SNR maintained, and the benefit of MCAR is limited. However, in the jamming cases, the key issue that affects the reconstruction performance is lack of measurements. So raising the number of measurements enhances the recovery performance, and the improvement of MCAR over FAR is remarkable.

## V. Conclusion

This paper proposes a new frequency agile waveform and theoretically analyzes its properties. Compared with the traditional FAR, the proposed waveform transmits multiple carriers in each pulse, and the returns are received individually. By exploiting the sparsity of the radar scene, CS methods are applied to process the radar echoes. Based on CS theories, the mutual coherence property of the measurement matrix is analyzed. The result shows that the proposed radar scheme promises to recover at least $K = O\left(\sqrt{\frac{NP}{\ln MN}}\right)$ scatterers, which is larger than $O\left(\sqrt{\frac{N}{\ln MN}}\right)$, the counterpart of the traditional FAR. Simulation results also validate the advantage of MCAR, especially when radar encounters jams.

## References

[1] S. R. J. Axelsson, "Analysis of random step frequency radar and comparison with experiments," *IEEE Transactions on Geoscience and Remote Sensing*, vol. 45, no. 4, pp. 890–904, 2007.

[2] Y. Liu, H. Meng, G. Li, and X. Wang, "Range-velocity estimation of multiple targets in randomised stepped-frequency radar," *Electronics Letters*, vol. 44, no. 17, pp. 1032–1034, 2008.

[3] T. Huang, Y. Liu, G. Li, and X. Wang, "Randomized stepped frequency ISAR imaging," in *Radar Conference (RADAR), 2012 IEEE*, May 2012, pp. 0553–0557.

[4] T. Huang, Y. Liu, H. Meng, and X. Wang, "Cognitive random stepped frequency radar with sparse recovery," *Aerospace and Electronic Systems, IEEE Transactions on*, vol. 50, no. 2, pp. 858–870, April 2014.

[5] J. Yang, J. Thompson, X. Huang, T. Jin, and Z. Zhou, "Random-frequency SAR imaging based on compressed sensing," *Geoscience and Remote Sensing, IEEE Transactions on*, vol. 51, no. 2, pp. 983–994, Feb 2013.

[6] D. Cohen, K. V. Mishra, and Y. C. Eldar, "Spectrum sharing radar: Coexistence via xampling," *IEEE Transactions on Aerospace and Electronic Systems*, pp. 1–1, 2017.

[7] T. Huang and Y. Liu, "Compressed sensing for a frequency agile radar with performance guarantees," in *2015 IEEE China Summit and International Conference on Signal and Information Processing, ChinaSIP 2015 - Proceedings*, 2015.

[8] Y. Liu, H. Meng, H. Zhang, and X. Wang, "Eliminating ghost images in high-range resolution profiles for stepped-frequency train of linear frequency modulation pulses," *IET Radar, Sonar Navigation*, vol. 3, no. 5, pp. 512–520, Oct 2009.

[9] Y. Liu, T. Huang, H. Meng, and X. Wang, "Fundamental limits of HRR profiling and velocity compensation for stepped-frequency waveforms," *IEEE Transactions on Signal Processing*, vol. 62, no. 17, pp. 4490–4504, Sept 2014.

[10] Y. C. Eldar and G. Kutyniok, *Compressed Sensing: Theory and Applications*. Cambridge University Press, 2012.

[11] T. Cai, L. Wang, and G. Xu, "Stable recovery of sparse signals and an oracle inequality," *Information Theory, IEEE Transactions on*, vol. 56, no. 7, pp. 3516–3522, July 2010.

[12] M. Grant and S. Boyd, "CVX: Matlab software for disciplined convex programming, version 2.1," http://cvxr.com/cvx, Mar. 2014.

[13] ——, "Graph implementations for nonsmooth convex programs," in *Recent Advances in Learning and Control*, ser. Lecture Notes in Control and Information Sciences, V. Blondel, S. Boyd, and H. Kimura, Eds. Springer-Verlag Limited, 2008, pp. 95–110, http://stanford.edu/~boyd/graph_dcp.html.